Discovery of new embedded Herbig-Haro objects in the ρ Ophiuchi dark cloud[*]

N. Grosso[1], J. Alves[2], R. Neuhäuser[1], and T. Montmerle[3]

[1] Max-Planck-Institut für extraterrestrische Physik, P.O. Box 1312, D-85741 Garching bei München, Germany
[2] European Southern Observatory Karl-Schwarzschild-Str. 2, D-85748 Garching bei München, Germany
[3] Service d'Astrophysique, CEA Saclay, F-91191 Gif-sur-Yvette, France

Abstract. We report here the discovery of a $30''$-chain of embedded Herbig-Haro (HH) objects in the ρ Ophiuchi dark cloud. These HH objects were first detected during a deep K_S-band observation (completeness magnitude for point source$\sim$19) made with NTT/SOFI. We confirm their nature with follow-up observations made with H_2 v=1–0 S(1) narrow-band filter. We argue that they belong to two different jets emanating from two Class I protostars: the main component of the recently resolved subarcsecond radio binary YLW15 (also called IRS43), and IRS54. We propose also to identify the [S II] knot HH224NW1 (Gómez et al. 1998) as emanating from a counterjet of YLW15. The alignment between these HH objects and the thermal jet candidate found in YLW15 by Girart et al. (2000) implies that this jet is not precessing at least on timescale $\sim$(2–4)$\times 10^4$ yr.

1. Introduction

In the 1950's, objective prism surveys of dark clouds revealed optical small nebulae, associated with young stars, showing emission line spectra with very weak continua. Today, these Herbig-Haro (HH) objects are interpreted as shocks produced by the interaction of outflows from Young Stellar Objects (YSOs) and the interstellar medium (see review by Reipurth & Raga 1999).

The ρ Ophiuchi dark cloud is one of the nearest (d$\sim$140 pc) active site of low-mass star formation, displaying a rich embedded cluster of $\sim$200 YSOs (see the updated census by the ISOCAM survey; Bontemps et al. 2001). It is thus one of the most suitable locations for the search of HH objects. Optical emission-line surveys (Hα, [S II]) have led to the detection of only 10 bona fide HH objects (Reipurth & Graham 1988; Wilking et al. 1997; Gómez et al. 1998; Reipurth 1999). As outlined by Wilking et al. and Gómez et al., most of these HH objects are located at the periphery of the cloud, in the lowest extinction area: optical surveys do not have access to embedded HH objects. Wilking et al. (1997) noted for all these neb-

ulae a relatively high [S II]/Hα ratio, which is a tracer of low excitation conditions, and thus indicates that H_2 is not destroyed after the bow shock; they suggested to use the shocked-H_2 transition at λ=2.121 μm to probe deeply embedded HH objects. Up to now in the ρ Ophiuchi dark cloud, shocked-H_2 imaging was only performed to study molecular shocks in the CO outflow of the Class 0 protostar prototype VLA1623 (e.g., Davis & Eisloeffel 1995), which led to the detection of several H_2-knots; one of them was later detected in [S II] (HH313; Gómez et al. 1998).

We report here deep near-IR observations of the ρ Ophiuchi dark cloud unveiling bow-shape structures and knots, and complementary observation with narrow-band filter confirming their nature as H_2 shocks. As these objects are not optically visible, we called them *embedded* HH objects, and discuss the possible exciting sources.

2. Observations and results

During the period April 4–7 2001, deep J, H, K_S-band observations of the ρ Ophiuchi dark cloud were made by N.G. with NTT/SOFI, as follow-up of Chandra and XMM-Newton X-ray observations. The complete report of this follow-up, consisting of 5 pointings, will be published in an upcoming paper (Grosso et al., in preparation). We will focus here only on the pointing related to the detection of
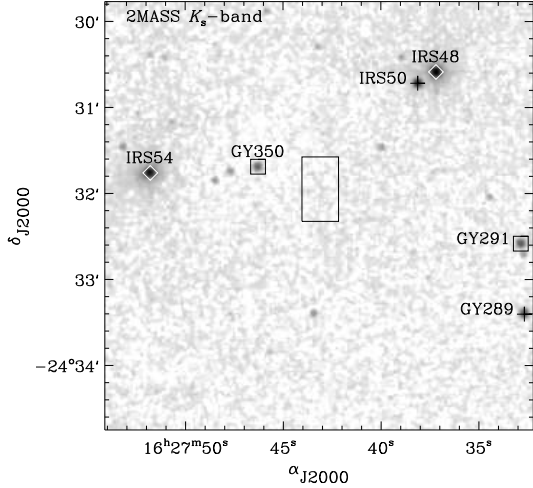
Fig. 1. K_S-band finding chart based on 2MASS survey image, showing the NTT/SOFI pointing field of view. The YSOs of this area are marked according to their IR classifications (diamond/square/cross for *resp.* Class I/II/III IR source; see Lada 1991) from the ISOCAM mid-IR survey (Bontemps et al. 2001). The box indicates the area enlarged in Fig. 2a.

new embedded HH objects, and located SE of the millimetric dense core Oph-B2 (Motte et al. 1998; see Fig. 1). This area was already surveyed by optical emission-line surveys, but no HH objects were found.

We used the auto jitter imaging mode to obtain a total integration time of 40 mn, with 6 s detector integration time (DIT) and 1 mn-exposure frames. The near-IR standard AS29-1 (Hunt et al. 1998) was observed several times during the night. We took five 6 s-darks at the end of the night. The different stages of the usual IR data reduction, namely sky estimation and subtraction, frame recentering and stacking, including also dark substraction and flat-field division (we used the flat-field provided by the NTT team for our observational period), were performed using the `jitter` routine of the ESO's `eclipse` package (version 3.8-1). Zero order astrometric correction was applied using the 2MASS field stars (Cutri et al. 2000) as reference frame, reducing the offset residual to $0.7''$. The magnitude zero-point was obtained from our calibration star.

Fig. 2a is an enlargement of the observation obtained with the K_S broad-band filter ($\lambda=2.162\,\mu$m, $\Delta\lambda=0.275\,\mu$m), unveiling a complex object showing bow-shape structures and possible emission knots. To detect weak structures in the J and H-band images, we filtered it with the wavelet transform (`MR/1` package; Starck et al. 1998) to a 5σ significance threshold. In this manner, a few of knot candidates are also detected in the H-band, and only one is detected in the J-band. The shape of this complex object is reminiscent of the ones found in HH objects. If this HH object interpretation is correct, this K_S-band detection must be mainly due to the $2.121\,\mu$m-line of the H_2 shocked emission. To confirm it, J. A. made a 20 mn-exposure observation (DIT=30 s, 1 mn-exposure frames) with NTT/SOFI using the H_2 v=1–0 S(1) narrow-band filter ($\lambda=2.124\,\mu$m, $\Delta\lambda=0.028\,\mu$m) during the night

of June 8 2001 (Fig. 2.b). The flat-field was computed from the median of the dark substracted frames. The good seeing conditions (FWHM$\sim0.7''$) of this shorter observation gives much more details than the K_S-band image.

To differentiate between pure line emission knots and continuum emission from stars (including scattered light) we follow Davis & Eisloeffel (1995) who noted that the narrow-band filter reduces the intensity of the field stars by the ratio of the filter bandpasses (~10), whereas the intensity of the H_2 knots is only reduced by ~2 (indeed spectra of H_2 molecular shocks have other emission lines in the K_S-band; see Smith 1995). We scale down the K_S-band image by the ratio of the filter bandpasses and the ratio of the seeing to have continuum features appearing with the same brightness in Fig. 2a and 2b. On the other hand, H_2-shocks appear ~5 times brighter in Fig. 2b than in Fig. 2a and can thus be easily identified. The H_2-knots detected are labelled on the H_2 contour map (Fig. 2c). Table 1 gives the position of these knots with photometry for a $1''$-aperture from the 5σ-filtered images. Before applying wavelet filtering the H_2 image was convolved with a Gaussian filter to have the same seeing as in the K_S-band image. To obtain the H_2 magnitudes, we scaled up the H_2 intensities by the filter-band width ratio and applied the magnitude zero-point of the K_S image.

The knots A display a bow-shape structure, characteristic of low-speed bow-shocks which produce such arcs and limb-brightened structures of conical appearance (Smith 1991). We also note in the H_2 image some diffuse emission downstream of the bow-shock which may be related to the excitation of H_2 in the pre-shock region of a J-shock. We thus propose the knots A as the leading part of a jet coming from the SW direction, and outlined by the upstream knots B. By contrast the knots C are displaced from the direction of this jet, and moreover the knots C_1–C_4 are clearly elongated, roughly along a NS direction. We propose to explain these features by shocks coming from the East and producing the arc C_2-C_1-C_5, with the downstream knots C_3 and C_4. We will discuss in the following section the possible exciting sources of these two jets.

To obtain an estimate of the H_2-shock velocity we compare the observed near-IR photometry with the predictions for planar molecular shocks (Smith 1995). We update first these results for the NTT set of filters. We extract the filter transmission profiles from the plots provided on the SOFI web page, and convolve them to the unfiltered molecular shock line fluxes (Michael D. Smith, private communication). Zero points for $J-H$ and $H-K_S$ colors are derived by requiring the colors of A0 spectrum template (Pickles 1998) to be zero. We observe f(K_S)/f(H_2)~1.4 and ~2.0 for the leading part of the two jets, which must be compared to f(K_S)/f(H_2)=2.0–3.3 (*resp.* 1.9–3.3) for J-shocks (*resp.* C-shocks) with velocity range 8–22 km s^{-1} (*resp.* 20–45 km s^{-1}). This implies J-shock (*resp.* C-shock) velocity ≤10 km s^{-1} (*resp.* 20 km s^{-1}), well below the H_2 dissociation velocity in molecular cloud (~22, ~47 km s^{-1} for *resp.* J, C-shock; see Smith 1995). Hence, the H_2-line emission is really map-
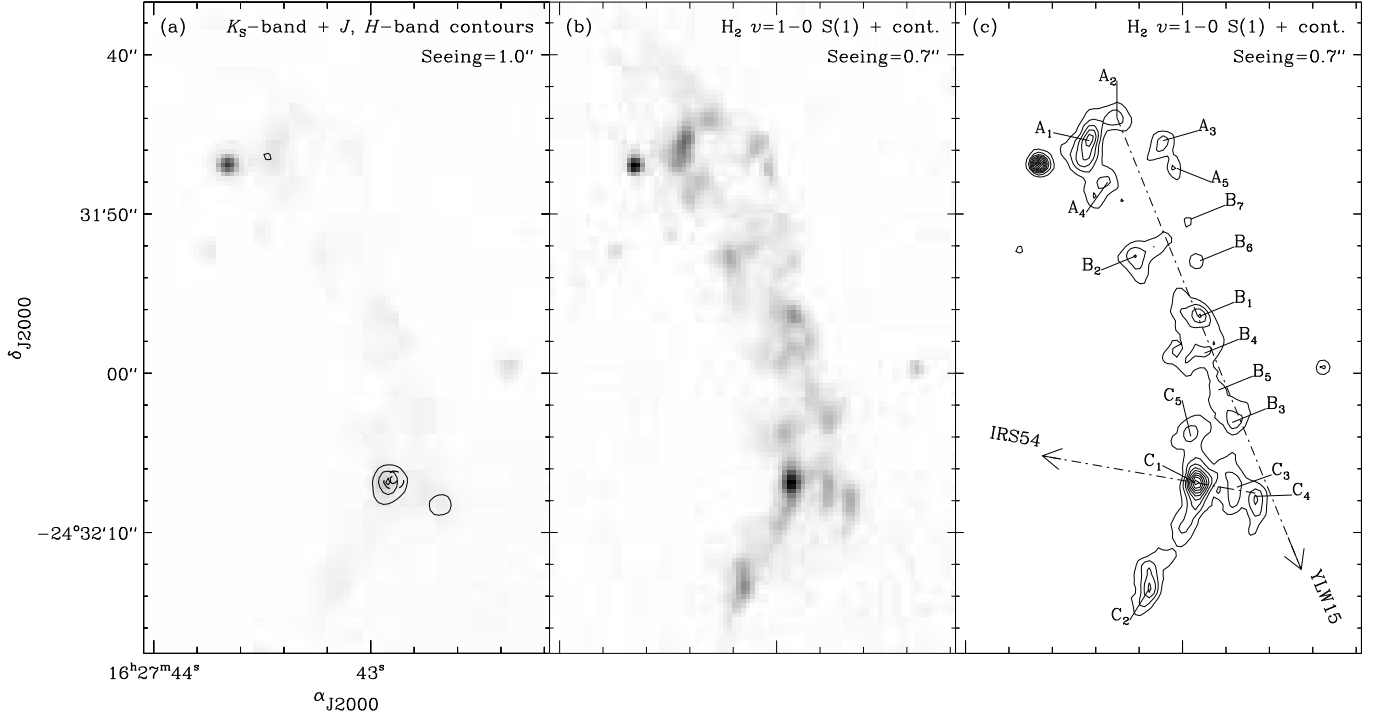
Fig. 2. Deep near-IR images of the embedded HH objects discovered with NTT/SOFI. (a) K_S-band image scaled so that continuum features from stars appear as bright as in the H_2 v=1–0 S(1) narrow-band filter image. The pixel size is $0''.29$, and the grey color scale is linear. J-band (*resp.* H-band) detections above 5σ levels are shown with dashed (*resp.* continuous) contour levels (24.5, 23.5, 23.0 and 21.8, 21.2, 20.9 mag arcsec^{-2}). (b) H_2 v=1–0 S(1) narrow-band filter image (including the continuum emission). H_2 line emission features appear brighter in this narrow-band image than in the previous broad-band one. (c) H_2 v=1–0 S(1) contour map (18.3, 17.6, 17.2, 16.9, 16.6, 16.5, 16.3, 16.1, 16.0, 15.9 mag arcsec^{-2}). The H2-knots are labeled by decreasing H_2 magnitudes (see Table 1). The first (*resp.* second) arrow joins the barycenter of the knots A–B (*resp.* C) and the Class I protostar YLW15 (*resp.* IRS54). The first arrow corresponds also to the symmetry axis of the knots A–B.

ping the bow-shock; we can exclude the scenario where this emission would come only from the low-velocity wing of a fast dissociative bow-shock located downstream, with strong iron lines in the J and H bands tracing the apex. These low-velocity embedded H_2-shocks are reminiscent

Table 1. H_2-knot positions and magnitudes.

Knot names	α_{J2000} 16^h27^m	δ_{J2000} $-24°$	J [mag]	H [mag]	K_S [mag]	H_2 [mag]	$\frac{f(K_S)}{f(H_2)}$
A_1	$43^s.4$	$31'45''.4$	–	23.7	19.3	17.1	1.4
A_2	$43^s.3$	$31'44''.0$	–	–	20.1	17.9	1.3
A_3	$43^s.1$	$31'45''.4$	–	–	20.3	18.1	1.2
A_4	$43^s.0$	$31'47''.1$	–	–	20.2	18.1	1.4
A_5	$43^s.4$	$31'48''.0$	–	–	20.9	18.6	1.1
B_1	$42^s.9$	$31'56''.4$	–	–	19.7	17.6	1.4
B_2	$43^s.2$	$31'52''.7$	–	–	20.0	17.7	1.2
B_3	$42^s.8$	$32'03''.1$	–	–	19.9	17.8	1.5
B_4	$42^s.9$	$31'58''.7$	–	–	20.0	17.9	1.4
B_5	$42^s.8$	$32'01''.1$	–	–	20.6	18.4	1.3
B_6	$42^s.9$	$31'52''.9$	–	–	21.8	18.8	0.6
B_7	$43^s.0$	$31'50''.3$	–	–	21.8	19.0	0.7
C_1	$43^s.0$	$32'06''.9$	24.5	21.2	18.5	16.6	1.7
C_2	$43^s.2$	$32'13''.5$	–	–	19.6	17.5	1.4
C_3	$42^s.7$	$32'07''.7$	–	–	19.6	17.8	2.0
C_4	$42^s.8$	$32'07''.2$	–	22.2	19.7	17.8	1.8
C_5	$43^s.0$	$32'04''.0$	–	–	20.0	17.9	1.4

of the low excitation HH objects already observed in the optical in this dark cloud. From the intrinsic color of low-velocity H_2-shocks, $(J-H)_0\sim0.8$, and assuming the reddening law quoted by Cohen et al. (1981), we estimate the extinction for knot C_1: A_V=9.09×[$(J-H)$-$(J-H)_0$]$\sim$23. This large visual extinction explains the non-detection by previous optical surveys. It will be possible to measure directly A_V by J, H-band spectroscopy using [Fe II] lines at 1.25 μm, 1.64 μm, which arise from the same atomic upper level.

3. Discussion on the exciting sources

The optical survey of HH objects in Taurus has shown that their frequency decreases rapidly with the age of the YSO, from Class I sources to Class II sources (Gómez et al. 1997), i.e. from evolved protostars to classical T Tauri stars. This result is consistent with the decrease of the CO outflows observed from the Class 0 sources to the Class I sources (Bontemps et al. 1996). To find the exciting source candidates of the HH objects reported here, it is thus reasonable to look for YSOs with IR excesses. On the basis of the HH feature morphology, we proposed in the previous section shocks coming from the East (*resp.* SW) to explain the shape of knots C (*resp.* A–B). We checked by constructing a color-color diagram of the sources detected

in our deep observation, that there is no new embebbed YSO with IR excess in these directions. Two known YSOs are Eastward (see Fig. 1): the Class II source GY350, and the Class I protostar IRS54. We propose to associate knots C with IRS54, the agreement with the knots C shape looking better (see Fig. 2.c). Strong H_2 v=1–0 S(1) line emission was detected in the IRS54 spectrum (Greene & Lada 1996), it is unresolved in our H_2 image, which shows only scattered light Eastward. To our knowledge this source has never been included in a CO outflow survey.

Fig. 2.c shows that the Class I protostar YLW15, also called IRS43, is on-axis of the knots A–B, $\sim$10′ away (0.4 pc for d=140 pc). This evolved protostar is a radio source, and was recently announced to be a subarcsecond radio binary (Girart et al. 2000). The main radio component, YLW15-VLA1, is spatially extended with a position angle of $25°\pm2°$(one sigma error), and Girart et al. proposed it to be a thermal radio jet candidate. The position angle (PA) of the knot chain, 22.3°, is compatible with the PA of this jet candidate within errors (Fig. 3). As the probability for a coincidence by chance between these PAs is very low $(2\times1.645\times2°/180°\approx0.037)$, the identification of YLW15 as the exciting source of knots A–B is likely. Fig. 3 displays the position of the HH objects of this dark cloud. The [S II] knot HH224NW1 (Gómez et al. 1998) was associated with the complex HH object HH224. We note however that HH224NW1 is displaced from the axis of HH224, and that the PA of YLW15 is 23.4°, thus also compatible with the orientation of the thermal jet candidate. HH224NW1 may then be related to a counterjet of YLW15. This association between YLW15 and these HH objects strengthens the proposal of Girart et al. for a ther-mal jet in this object. Moreover the alignment with the HH objects moving at $V \leq$10–20 km s^{-1} implies that this jet is not precessing at least on timescale $\sim(2–4)\times10^4$ yr.

These observations confirm that HH objects excited by Class I protostars may be hidden by large extinctions in the optical, but can be easily unveiled and studied by deep near-IR observations. Embedded HH objects are probably very common, and it is essential now to obtain a reliable census, for instance to quantify the role of outflows in maintaining a high level of turbulence in molecular clouds and regulating star formation (Matzner & McKee 2000).

References

Bontemps, S., André, P., Terebey, S., & Cabrit, S. 1996, A&A 311, 858

Bontemps, S., André, P., Kaas A. A., et al. 2001, A&A 372, 173

Cohen, J. G., Persson, S. E., Elias, J. H., & Frogel, J. A. 1981, ApJ 249, 481

Cutri, R., Skrutskie, M.F., Van Dyk, S., et al. 2000, http://www.ipac.caltech.edu/2mass/releases/-second/doc/explsup.html

Davis, C. J. & Eisloeffel, J. 1995, A&A 300, 851

Girart, J. M., Rodríguez, L. F., & Curiel, S. 2000, ApJ 544, L153

Gómez, M., Whitney, B. A., & Kenyon, S. J. 1997, AJ 114, 1138

Gómez, M., Whitney, B. A., & Wood, K. 1998, AJ 115, 2018

Greene, T. P. & Lada, C. J. 1996, AJ 112, 2184

Hunt, L. K., Mannucci, F., Testi, L., et al. 1998, AJ 115, 2594

Lada, C. J. 1991, in The Physics of Star Formation and Early Stellar Evolution, NATO ASI, C.J. Lada & N.D. Kylafis (eds.), Kluwer, p. 329

Matzner, C. D. & McKee, C. F. 2000, ApJ 545, 364

Motte, F., André, P., & Neri, R. 1998, A&A 336, 150

Pickles, A. J. 1998, PASP 110, 863

Reipurth, B. 1999, A General Catalogue of Herbig-Haro Objects (2nd ed.), http://casa.colorado.edu/hhcat

Reipurth, B. & Graham, J. A. 1988, A&A 202, 219

Reipurth, B. & Raga, A. C. 1999, NATO ASIC Proc. 540: The Origin of Stars and Planetary Systems, p. 267–304

Smith, M. D. 1991, MNRAS 252, 378

Smith, M. D. 1995, A&A 296, 789

Starck, J.-L., Murtagh, F., Bijaoui, A. 1998, Image Processing and Data Analysis: The Multiscale Approach, Cambridge Univ. Press, Cambridge (UK)

Wilking, B. A., Schwartz, R. D., Fanetti, T. M., & Friel, E. D. 1997, PASP 109, 549
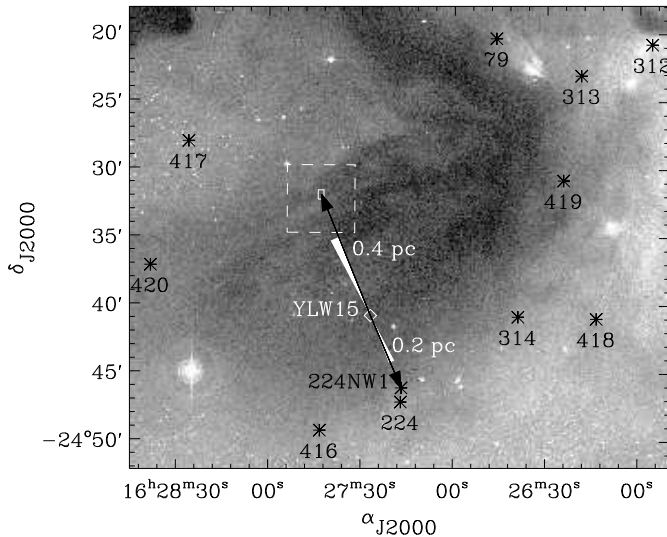
Fig. 3. Optical finding chart (DSS2-red) of the HH objects in the ρ Ophiuchi dark cloud. The numbers refer to the HH object list of Reipurth (1999). The dashed square shows the NTT/SOFI field of view. The position of the new embedded HH objects is marked by the white box. The white sectors show the position angle of the thermal jet candidate of the Class I protostar YLW15 including 90% error level (Girart et al. 2000).